An Overview of Dynamic Causal Modeling

Valerie Bradley, Ana Ignatieva, Yuxi Jiang and William Thomas

January 2019

1 Introduction

Dynamic Causal Models (DCMs) are generative models widely used to characterize effective connectivity of neurons in the brain, linking neuronal activity to responses observed in functional MRI (fMRI) and electromagnetic time series (EEG and MEG) data. Since the introduction of the original bilinear model by Friston et al. (2003), numerous extensions to the model have been proposed to better reflect neuronal behaviour and interactions between neurons. One such extension is a class of non-linear dynamic causal models, proposed by Stephan et al. (2008).

Within this report, we will examine the role of bilinear and non-linear DCMs in neuroimaging, as well as some wider applications and generalisations of Bayesian dynamic networks. In Section 2, we begin by describing the theory of linear and non-linear DCMs, including their construction, fitting and model selection. In Section 3, we replicate some of the results obtained by Stephan et al. (2008), before moving on to explore a broader class of Bayesian dynamic networks in Section 4. Finally, we present a discussion of the limitations and potential extensions of both DCMs and Bayesian networks in Section 5.

2 Theory of Dynamic Causal Models

In a neurological setting, DCMs seek to infer processes and mechanisms at a neuronal level, using measurements of brain activity. That is, they seek to model connectivity between different regions of the brain and explore how this connectivity is affected by external stimuli. To do this, the full forward model is composed of a neuronal equation, describing the hidden neuronal dynamics, as well as a set of hemodynamic equations, describing how changes in the neuronal system are translated into observed responses.

The original model proposed by Friston et al. (2003) made use of a bilinear approximation to the function governing the neuronal dynamics, but more recently, Stephan et al. (2008) proposed a non-linear approximation to account for additional neuronal processes. In particular, the non-linear framework allows us to model "gating" of connections between neurons, where connections between neurons are enabled by activity in other regions of the brain. While non-linear processes such as gating are absent from the bilinear framework, there are arguments for omitting the non-linearities. For example, fMRI records responses of large neuronal populations, whose ensemble activity is well characterised by linear approximations. There is also reason to believe that some non-linear information is lost when passed through the hemodynamic equations, which have low-pass filtering properties. Because of this, we will introduce the framework for both sets of DCMs, acknowledging that different models may be more appropriate in certain situations.

2.1 Neuronal equation

The neuronal state equation proposed by Friston et al. (2003) estimates effective connectivity using a function of the neuronal states of other brain regions. Let $x = (x_1, \ldots, x_n)$ be a vector of the neuronal states containing neuronal population activity of each region; and $u = (u_1, \ldots, u_m)$ be a vector describing the experimentally controlled (known) inputs into the system. Under the assumption that all the processes

are deterministic and occur instantaneously, the changes in state activities can then be represented by the differential equation:

$$\frac{dx}{dt} = F(x, u, \theta), \tag{1}$$

where F is some nonlinear function that is able to describe the neurophysiological influences exerted by the input u and activity x upon changes in the others, and θ is a parameter vector that controls the strength of influences between the states.

Equation (1) can then be approximated using Taylor series. After reparameterisation, the bilinear form (Friston et al., 2003) and nonlinear form (Stephan et al., 2008) of the Taylor series approximation to equation (1) can be easily interpreted in terms of effective connectivity.

Bilinear form

$$\begin{aligned} F(x, u, \theta) &\approx \frac{\partial F}{\partial x}x + \frac{\partial F}{\partial u}u + \frac{\partial^2 F}{\partial x \partial u}xu \\ &= (A + \sum_{i=1}^{m} u_i B^{(i)})x + Cu \end{aligned}$$

where matrix $A = \frac{\partial F}{\partial x}$ describes the fixed strength of connection between the different regions when there is no input into the system; matrices $B^{(i)} = \frac{\partial^2 F}{\partial x \partial u_i}$ represent the additional changes in the strength of connections introduced by the i^{th} input; and matrix $C = \frac{\partial F}{\partial u}$ is the direct influences of the inputs on neuronal activities.

Nonlinear form

$$\begin{aligned} F(x, u, \theta) &\approx \frac{\partial F}{\partial x}x + \frac{\partial F}{\partial u}u + \frac{\partial^2 F}{\partial x \partial u}xu + \frac{1}{2}\frac{\partial^2 F}{\partial x^2}x^2 \\ &= (A + \sum_{i=1}^{m} u_i B^{(i)} + \sum_{j=1}^{n} x_j D^{(j)})x + Cu \end{aligned}$$

where matrices $D^{(j)} = \frac{1}{2}\frac{\partial^2 F}{\partial x_j^2}$ explain the effect activity in region j has on the strength of responses from the regions to different inputs. The additional second order term of the state vector from the Taylor series approximation included in the nonlinear form can be used to describe the effect of neuronal gain, where the response of a given neuron to an input depends on the history of inputs the neuron previously received from other different neurons.

2.2 Hemodynamic equation

The second part of a DCM consists of a set of hemodynamic differential equations, which govern the relationship between the neuronal states and the observed responses. These describe how vasodilation s, blood flow f, blood volume v and deoxyhemoglobin content q are linked to changes in neuronal population activity. The predicted blood oxygen level dependent (BOLD) signal can then be modelled as a non-linear function of v and q. While several different hemodynamic models exist, we will focus on the model used by Stephan et al. (2008), which was originally proposed by Stephan et al. (2007b). This consists of three main components:

1. Differential equations describing the link between neural activity and regional cerebral blood flow (rCBF).

2. Differential equations describing the dependence of BOLD signal on rCBF induced changes of blood volume v and deoxyhemoglobin content q.

3. The BOLD signal change equation linking v and q to BOLD signal change.

These equations are all described in detail in the appendix. Together, these equations completely specify the hemodynamic model and it can be used to predict BOLD signal. In practice, given inputs u and parameters θ, we model the measured BOLD signal y as the predicted BOLD signal $h(u, \theta)$, plus a linear mixture of confounding variables $X\beta$ and some Gaussian observation error ε:

$$y = h(u, \theta) + X\beta + \varepsilon.$$

2.3 Parameter Estimation

To estimate the parameters for the non-linear model, Stephan et al. (2007a) use a Bayesian procedure, based on zero-mean shrinkage priors for the coupling parameters (A, B, C and D) and empirical priors for the hemodynamic parameters (s, f, v and q). The choice of the coupling priors is motivated by the necessary constraints imposed by neuronal dynamics, while the empirical priors for hemodynamic parameters are relatively easy to specify. In particular, the hemodynamic parameters are taken to have Gaussian priors, where the prior means and variances are posterior estimates obtained from single subject fMRI time series, as described in Friston (2002). While these priors are informative, no inferences are made regarding the hemodynamic parameters.

On the other hand, one of the main prior constraints for the coupling parameters stems from the fact that neuronal systems need to remain stable in the absence of any input. This can be imposed using Gaussian priors for the coupling parameters, constraining them such that the principal Lyapunov exponents for A and B are both negative. When these are negative, the system will converge to a point attractor. In particular, the priors for a_{ij} and b_{ij}^k are taken to be i.i.d. Gaussian with mean 0 and prior variance v_a. The priors for c_{ik} are taken to be uninformative with mean 0 and variance 1. While we make inferences regarding the coupling parameters, here the priors have all been taken to be relatively flat.

The conditional density $p(\theta|y)$ is first approximated using a fixed-form Laplace approximation, under which the density assumes a Gaussian form. The posterior moments of the parameters can then be iteratively updated through the variational Bayes approach; where the variational modes can be updated using gradient ascent on the free-energy, which is a lower bound of the log-evidence of the model. Detailed explanation of this approach can be found in Friston et al. (2007).

2.4 Bayesian Model Selection (BMS)

In order to make model comparisons, Stephan et al. (2007a) use Bayesian model selection. This involves maximising the model evidence $p(y|m)$, for measurements y and a model m. In particular, an approximation to the log-evidence is used, which involves the variational free energy F:

$$F = \log p(y|m) - KL[q(\theta), p(\theta|y, m)].$$

Here, $q(\theta)$ represents the approximating posterior density, $p(\theta|y, m)$ represents the true posterior density and $KL[q(\theta), p(\theta|y, m)]$ denotes the Kullback-Leibler divergence between the two densities. This gives a measure of dissimilarity between the two densities, which if minimised, tells us that $q(\theta) \approx p(\theta|y, m)$ and hence, $F \approx \log p(y|m)$. The Kullback-Leibler divergence is minimised after parameter estimation, so we are able to make model comparisons by considering differences in log-evidence or by using Bayes factors. Given models m_i and m_j, the Bayes factor is of the form

$$BF_{ij} = \frac{p(y|m_i)}{p(y|m_j)} \approx \exp(F_i - F_j).$$

3 Examples

3.1 Replicating results of Stephan et al. (2008)

We used the SPM12 MATLAB software and available data[1] to replicate the results of Stephan et al. (2008). The manual (Ashburner et al., 2014) contains detailed instructions on specifying and fitting DCMs.

We fit all four models ("M1" through "M4") as illustrated in Figure 6 of the original paper by Stephan et al. (2008). We kept all inputs and connections the same as described by the authors (although details such as the location of the regions of interest were not explicitly stated in the paper, so the values given in the SPM12 manual were used). The fits of the bilinear model (M3) and nonlinear model (M4) to the data are shown in Figure 1. The data is shown as dotted lines; the fit of V1, V5 and SPC responses are shown as solid red, yellow and blue lines, respectively. The fits appear broadly similar to those demonstrated by Stephan et al. (2008); some differences are present in the values of the fitted parameters and the shapes of the fitted curves, but this could be due to different versions of the software used and the fitting method.

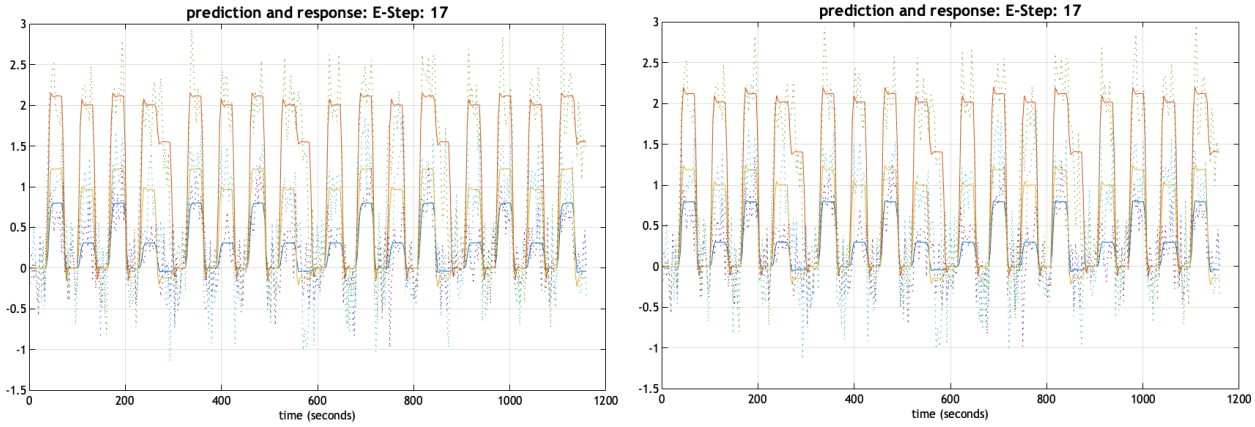

Figure 1: V1 (red), V5 (yellow) and SPC (blue) responses for the bilinear model (left) and the nonlinear model (right). The data is shown as dotted lines.

We also ran Bayesian model comparison on the four models using SPM12. We found that the nonlinear model provided the best fit for the data, agreeing with Stephan et al. (2008).

4 Generalisation

DCMs have been developed specifically for application to neurological data - the forward generative model is based on the underlying physiological dynamics of the brain. However, DCMs are simply a subset of nonlinear Dynamic Bayesian Networks where the nonlinear relationship between input data and observation data is structured such that parameters have specific neurological interpretations. Bayesian dynamic networks, and even more generally, Bayes networks, have far more widespread applications. In this section we will demonstrate the widespread applicability of Bayes networks by considering examples of applications to gene expression and polling datasets.

4.1 Dynamic Bayesian Networks for gene expression data

An example of an application of DBNs to genetic data is in modelling inter-dependencies in the regulatory pathways governing gene expression. Genes are contained within DNA strands as sequences of nucleotides. Gene expression refers to the process by which the genes are used to create specific substances (most

[1] Attention to visual motion fMRI data set available at `www.fil.ion.ucl.ac.uk/spm/data/attention`

commonly, proteins). Some genes are expressed more frequently than others; the regulation of gene expression by the cell is a complicated process comprising several mechanisms, which can interact with each other. In this setting, we are interested in studying the relationships between genes – e.g. whether expression of one gene influences the expression of another.

Using Bayesian networks in this context was first proposed by Friedman et al. (1998), and extended to the dynamic model by Ong et al. (2002). A simplified example of the model of gene regulation is shown in Figure 2. Hidden states (with no observable measurements) are shaded purple. Activator molecules act on operons, which control the expression of one or more genes; operons can interact over time and form feedback loops. The level of activity changes over time, with multiple measurements of gene expression being taken. The fitted parameters are the strengths of influence between any two operons, and between operons and genes.

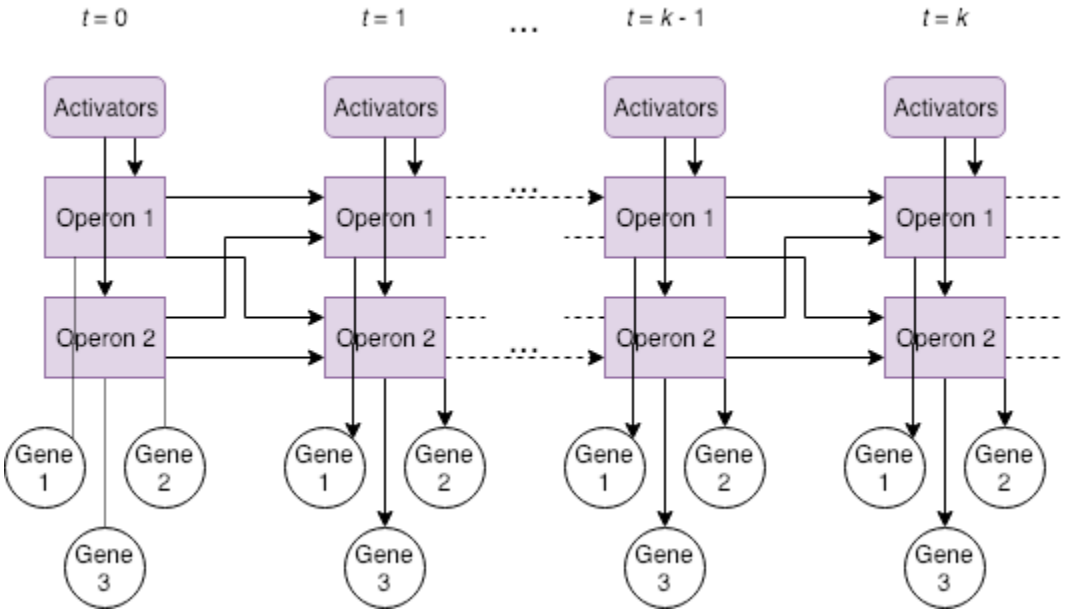

Figure 2: Example of a gene regulation model proposed by Ong et al. (2002).

Ong et al. (2002) use an EM algorithm to fit a full model to genomic data for *E. Coli*, and thus learn the structure of dependence. Their model offers a simplification of the regulatory process, for instance not accounting for external influences such as temperature, but nonetheless provides useful insights into the underlying processes.

4.2 Dynamic Bayes Networks for political polling

4.2.1 The data

The polling data we consider in this example are a series of polls conducted leading up to the 2016 US presidential election collected from FiveThirtyEight.com. The data includes 12,624 polls conducted by 42 different pollsters from January 1, 2016 through November 7, 2016. We limited the data to national (instead of state-specific) polls conducted after September 1, 2016 (after the nominees from each party had been selected) and to polls conducted by top pollsters or those who conducted at least 20 polls. These restrictions left 393 polls from 15 pollsters over the final 68 days before the election.

4.2.2 Normal model

In the first model, we used 2-way support for Hillary Clinton (HRC) (relative to Donald Trump (DJT)) on day $t = (1, ..., T)$ collected by pollster $k = (1, ..., K)$ as the observed variable, $Y_{t,k}$. We assumed the

observed data had the following distribution:

$$Y_{t,k} \sim \mathrm{N}(\theta_t + \mu_k, V/s_{t,k})$$

where μ_k is the bias of the k^{th} pollster and θ_t is the true proportion of the population that supports HRC on day t. The parameter $s_{t,k}$ represents the sample size of the poll, and V is a variance-scaling parameter shared across all polls. On the first day, $t = 1$, θ_1 is assumed to be distributed $\mathrm{N}(0.5, 0.05)$, a prior of about even support for HRC and DJT. Support for HRC on subsequent days is assumed to evolve as follows:

$$\theta_{t=(2,\ldots,T)} \sim \mathrm{N}(\theta_{t-1}, W_t)$$

It is important to note that not all pollsters conducted polls every day, so many of the $Y_{t,k}$ outcomes were not actually observed. This model is useful, but a vast simplification of the underlying process. The main oversight is that the outcome observed by pollsters is not 2-way support for the main candidates, but rather a distribution across at least 3 outcomes (HRC, DJT or "undecided"), and often more if third-party candidates are included in the response options. In order to more accurately represent the data generating process, a second model was also considered.

4.2.3 Dirichlet model

This model modifies the observation equation above to model the proportion of respondents in each poll who supported HRC, supported DJT, supported another candidate, or who were undecided. Additionally, some polls offered respondents third-party candidates as an option (4-way outcome) while others did not (3-way outcome). These were treated as separate outcomes $\boldsymbol{Y}_{M,t,k}$, where $M \in (3, 4)$ represents the number of outcomes offered to respondents. We assume that these two types of outcomes ($\boldsymbol{Y}_{3,t,k}$ and $\boldsymbol{Y}_{4,t,k}$) depend on the same underlying strength parameter, $\boldsymbol{\theta}_t$, which we now represent as a vector of the true distribution of support for each of the 4 outcomes across the population, $\boldsymbol{\theta}_t = (\theta_{t,1}, \theta_{t,2}, \theta_{t,3}, \theta_{t,4})$ where $\sum_{m=1}^{4} \theta_{t,m} = 1$. Similarly, we assume that the pollster biases, $\boldsymbol{\mu}_k$ are now vectors of length 4, with each element corresponding to the k^{th} pollster's likelihood of over- or under-estimating a particular category (i.e. some pollsters ask questions in such a way that they systematically underestimate the undecided population). The full hierarchical model for observations is given by

$$\begin{aligned}
\boldsymbol{Y}_{4,t,k} &\sim \text{Dirichlet}(\boldsymbol{\theta}_t + \boldsymbol{\mu}_k) \\
\boldsymbol{Y}_{3,t,k} &\sim \text{Dirichlet}(\boldsymbol{\theta}_{t,m=1:3} + \boldsymbol{\mu}_{k,m=1:3}) \\
\boldsymbol{\theta}_{t=1} &\sim \text{Dirichlet}(0.44, 0.42, 0.1, 0.04) \\
\boldsymbol{\theta}_{t=(2,\ldots T)} &\sim \text{Dirichlet}(\boldsymbol{\theta}_{t-1}) \\
\boldsymbol{\mu}_k &\sim \boldsymbol{N}(0, \Sigma)
\end{aligned}$$

4.2.4 Results and Discussion

The models were fitted using rSTAN, each with 4 chains of 1000 warm-up and 1000 sampling iterations, suggested by (**?**. The left plot in Figure 3 shows the posterior mean and 50% HDI of θ_t over time. The fluctuation in θ_t matches that of the observed 2-way support of HRC of individual polls (represented as points). The actual support on election day ($t = T + 1$) for Hillary was 50.1%, within the 50% HDI estimated for θ_T.

The right plot in Figure 3 shows the results of the Dirichlet model. This model gives a richer picture of the true dynamics of support through the 2016 US presidential election cycle. As expected, rate of undecided voter and supporters of third party candidates drops steadily as election day approaches, however the model vastly overestimates third-party support at the expense of support for HRC and DJT. Interestingly, there is a drop in support for both HRC and DJT in the final days before election day, mirrored by a corresponding spike in support for third-party candidates and undecideds. This could

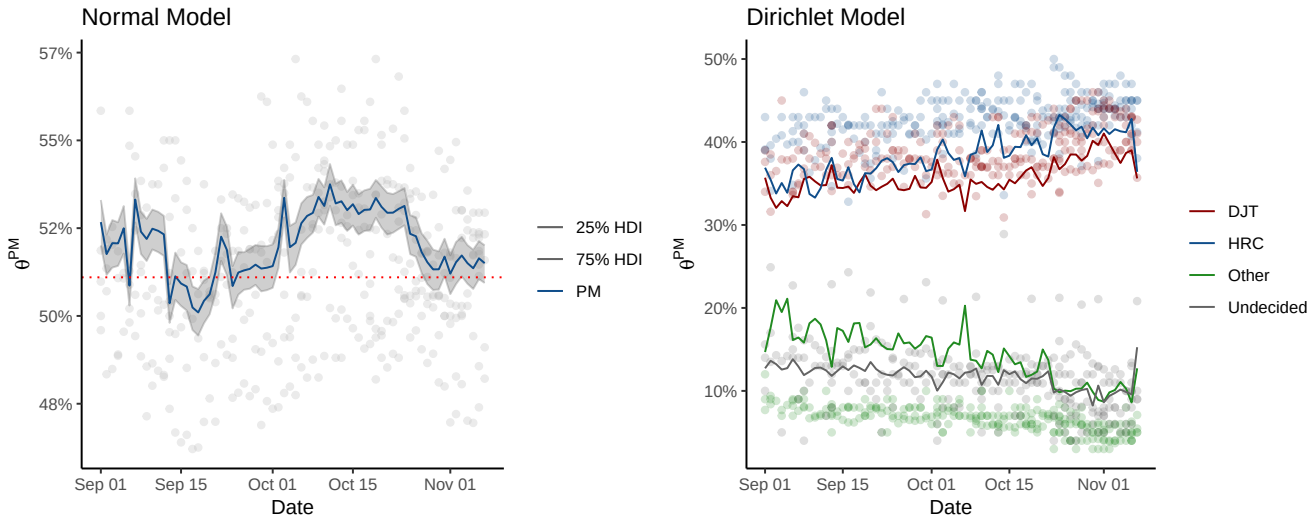

Figure 3: The plots show the posterior means of θ_t estimated from the Normal model (left) and the Dirichlet model (right) over time.

reflect changes in support following the release of the "Comey Letter". Complicating this hypothesis, however, is that the spike in support starts to materialize about a week after the letter was actually released. This begs the question of how long it takes the impact exogenous events to be reflected in polling data, since most polls are conducted over a series of 3-7 days. The results of the pollster bias analysis are presented in the appendix

The models presented here are the first step in applying DBNs to political polling data, and there are a vast number of opportunities to improve the models. First, the work here does not do any analysis of model fit beyond a simple "gut check" that the results produced are reasonable and the one-step forward prediction for election day was close to the actual outcome. A more robust analysis would perform Bayesian model selection, similar to that discussed in Stephan et al. (2008), and analyze the sensitivity of estimates to the particular priors and hyperpriors used. We also could have used cross-validation on a held-out training set to evaluate how well the models generalize to new data.

A second vein along which these models could have been improved involves the specification of the underlying data generating process. These models make a number of simplifying assumptions, that likely bias the results. These assumptions include: 1) that pollster error is uncorrelated with other pollsters (when we know that pollster "herding" is actually quite common), 2) that the process is stationary (when in fact it's clear that the proportion of support for third-party candidates decreases over time) and 3) that the polls are a snapshot of support at time t (when in fact they are usually measured over 3-7 days). Future models should account for these phenomena.

A final way in which these models could be improved and extended is by using them to estimate the impact of exogenous events (like the "Comey letter", the "Access Hollywood" tape, and presidential debates) on candidate support. More specifically, we could answer the following questions: 1) do these events have any impact, 2) how long does it take for that impact to manifest, 3) how does that impact manifest (i.e. by decreasing support for the candidate involved, by decreasing the likelihood that people will vote at all, which groups does the event impact, etc.) and 4) how long does that impact endure?

5 Discussion

DCMs are a novel approach to modelling fMRI data, taking into account both the neural dynamics and the hemodynamics in the brain. Through this, we are able to infer how different regions of the brain

are connected in response to external stimuli and how neuronal activation in one region of the brain can regulate connections between other regions. In replicating the results of Stephan et al. (2008), we have also demonstrated that the non-linear DCM has the ability to model some of the more complicated relationships between neurons. However, these models do have some shortcomings which prompt further research questions.

When it comes to model fitting, optimisation of the free energy can be difficult due to the presence of multiple local maxima. This can lead to bias in the approximate posterior densities and lead to inconsistent parameter estimates, making the reproducibility of results an issue (Daunizeau et al., 2011). There is also concern that model comparison is based upon a lower bound to the log-evidence, rather than on the model evidence itself. Daunizeau et al. (2011) note that the tightness of the bound scales with the resemblance between the true and approximate posterior densities, calling into question whether the Laplace approximation is problematic for model comparison.

Although Stephan et al. (2008) check the parameter estimation procedure through the use of simulated data, it is not entirely clear how well the models actually fit the observed data, or how fully the model describes the physiological reality. Using Bayesian model comparison it is evident that the non-linear model provides a better fit than the bilinear model, but there is limited discussion of model validation. There is also reason to believe that combining multiple data modalities, such as EEG and fMRI imaging data, could improve the model further, but the DCMs discussed are not equipped to handle this. Such an extension is proposed by Friston et al. (2017).

Finally, we note that DCMs for fMRI data are fitted to imaging data from a single individual (Friston et al., 2003; Friston, 2002; Stephan et al., 2007a). When it comes to making group-level inferences, we must consider methods for aggregating estimates across subjects. There are two main methods for group-level inference in the DCM context: Bayesian Parameter Averaging (BPA) and Bayesian Model Averaging (BMA) (Stephan et al., 2010). The choice of procedure should be motivated by the type of inferences desired, as well as hypotheses about the underlying function model, such as whether the parameters of interest are fixed or random effects. Extending the modelling to handle multiple observations may provide more robust inference.

We also considered a more general class of dynamic Bayesian network models. These models provide a flexible framework for capturing complex inter-dependencies within systems that evolve over time. We demonstrated the wide applications of DBNs with applications to genetics and political polling data.

References

Ashburner, J., Barnes, G., Chen, C., Daunizeau, J., Flandin, G., Friston, K., Kiebel, S., Kilner, J., Litvak, V., Moran, R. et al. (2014). SPM12 manual.

Daunizeau, J., David, O. and Stephan, K. (2011). Dynamic causal modelling: A critical review of the biophysical and statistical foundations. *NeuroImage*, **58**(2), 312 – 322.

Friedman, N., Murphy, K. and Russell, S. (1998). Learning the structure of dynamic probabilistic networks. In *Proceedings of the Fourteenth conference on Uncertainty in artificial intelligence*, pp. 139–147. Morgan Kaufmann Publishers Inc.

Friston, K., Mattout, J., Trujillo-Barreto, N., Ashburner, J. and Penny, W. (2007). Variational free energy and the Laplace approximation. *Neuroimage*, **34**(1), 220–234.

Friston, K., Preller, K. H., Mathys, C., Cagnan, H., Heinzle, J., Razi, A. and Zeidman, P. (2017). Dynamic causal modelling revisited. *Neuroimage*.

Friston, K. J. (2002). Bayesian estimation of dynamical systems: an application to fMRI. *Neuroimage*, **16**(2), 513–530.

Friston, K. J., Harrison, L. and Penny, W. (2003). Dynamic causal modelling. *Neuroimage*, **19**(4), 1273–1302.

Ong, I. M., Glasner, J. D. and Page, D. (2002). Modelling regulatory pathways in e. coli from time series expression profiles. *Bioinformatics*, **18**(suppl_1), S241–S248.

Stephan, K. E., Harrison, L. M., Kiebel, S. J., David, O., Penny, W. D. and Friston, K. J. (2007a). Dynamic causal models of neural system dynamics: current state and future extensions. *Journal of Biosciences*, **32**(1), 129–144.

Stephan, K. E., Kasper, L., Harrison, L. M., Daunizeau, J., den Ouden, H. E., Breakspear, M. and Friston, K. J. (2008). Nonlinear dynamic causal models for fMRI. *Neuroimage*, **42**(2), 649–662.

Stephan, K. E., Penny, W. D., Moran, R. J., den Ouden, H. E., Daunizeau, J. and Friston, K. J. (2010). Ten simple rules for dynamic causal modeling. *Neuroimage*, **49**(4), 3099–3109.

Stephan, K. E., Weiskopf, N., Drysdale, P. M., Robinson, P. A. and Friston, K. J. (2007b). Comparing hemodynamic models with DCM. *NeuroImage*, **38**(3), 387 – 401.

A Hemodynamic Model

Taking x to be the neuronal state vector, κ to be the rate constant of vasodilatory decay, γ to be the rate constant of flow-induced feedback regulation, τ to be the mean transit time of venous blood, a to be the resistance of the venous balloon and E_0 to be the resting oxygen extraction fraction, we are able to fully describe the hemodynamic model in terms of differential equations. The neurovascular state equations

$$\frac{ds}{dt} = x - \kappa s - \gamma(f-1), \qquad \frac{df}{dt} = s,$$

describe changes in vasodilatory signalling s and changes in blood flow f respectively, while the differential equations

$$\tau\frac{dv}{dt} = f - v^{1/\alpha}, \qquad \tau\frac{dq}{dt} = f\left[\frac{1-(1-E_0)^{1/f}}{E_0}\right] - v^{1/\alpha}\frac{q}{v},$$

describe changes in blood volume v and deoxyhemoglobin content q.

Taking ΔS to be the BOLD signal change, S_0 to be the resting BOLD signal and V_0 to be the resting venous blood volume fraction, the BOLD signal change equation is given by

$$\frac{\Delta S}{S_0} \approx V_0\left[k_1(1-q) + k_2\left(1-\frac{q}{v}\right) + k_3(1-v)\right],$$

where k_1, k_2 and k_3 are as specified in Stephan et al. (2007b).

B Pollster bias results

Figure 4 shows the sampled posterior distributions for both the Normal and Dirichlet models. The results presented for the Dirichlet model correspond to the first element of the $\boldsymbol{\mu}_k$ vector, or $\mu_{k,HRC}$. This element can be interpreted as the factor by which each pollster overestimates support for Clinton. The units and scale of the Dirichlet model u_ks is not as clear as those of the Norm model, in which each μ_k can be thought of as the number of percentage points by which each pollster overestimated support for Hillary Clinton.

The rank-ordering of pollsters in the Normal model is roughly in-line with pollster reputations. For example, ABC has one of the smallest biases, and is the only pollster in this data set to have been given an "A+" ranking by FiveThirtyEight. On the other end of the spectrum, Rasmussen is to favor Republicans and here is estimated to have one of the most-negative μs. The LA Times is estimated to have the most negative bias - a poll that received a high volume of attention during 2016 for consistently predicting higher support for Donald Trump than other polls.

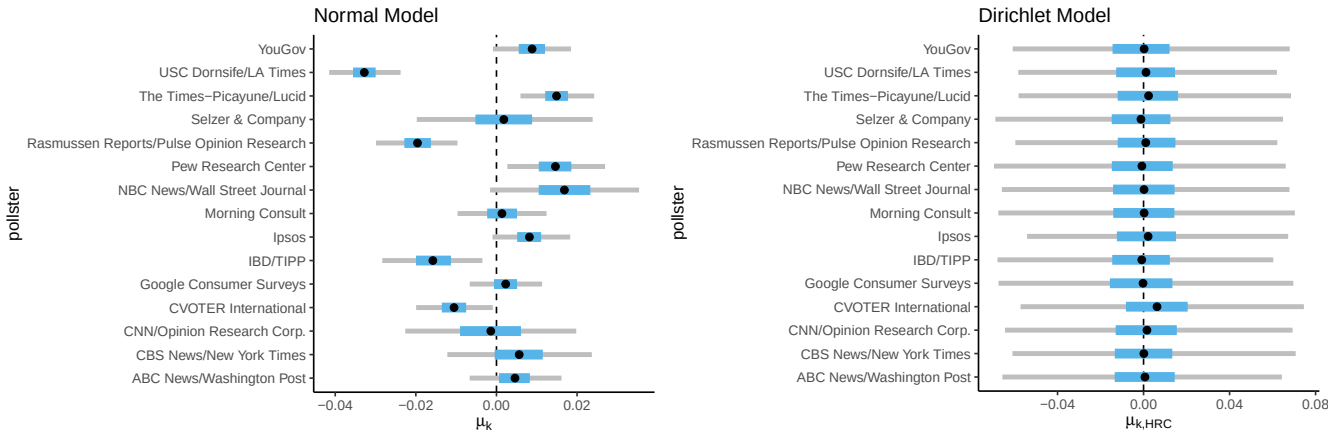

Figure 4: Posterior distributions of pollster bias parameters (μ_k) for the Normal model (left) and the Dirichlet model (right). The μ_k from the Dirichlet model correspond to the first bias parameter, $\mu_{k,HRC}$.